# Correlation between Density Functional Studies and Experimental Data of Three New 19-Electron Metal Sandwich Complexes Containing Amido, Ester, and Thioester Cyclopentadienyl Substituents

Samia Kahlal,[†] Cátia Ornelas,[‡] Jaime Ruiz,[‡] Didier Astruc,*[,‡] and Jean-Yves Saillard*[,†]

*Sciences Chimiques de Rennes, UMR CNRS No. 6226, Université de Rennes 1, 35042 Rennes Cedex, France, and Institut des Sciences Moléculaires, UMR CNRS No. 5255, Université de Bordeaux I, 351 Cours de la Libération, 33405 Talence Cedex, France*

*Received January 7, 2008*

Three 18-electron complexes of the type $[CpFe^{II}(\eta^6\text{-}C_6Me_6)]^+$ containing an amido, an ester, and a thioester group directly attached to the Cp ring were synthesized and reduced to $Fe^I$ 19-electron complexes. These new 19-electron stable complexes were characterized by UV/vis spectroscopy, showing significant differences in the obtained spectra. In order to better understand the structural and optical properties of the three 19-electron complexes $(\eta^5\text{-}C_5H_4CONHR)Fe^I(\eta^6\text{-}C_6Me_6)$, $(\eta^5\text{-}C_5H_4COOR)Fe^I(\eta^6\text{-}C_6Me_6)$, and $(\eta^5\text{-}C_5H_4COSR)Fe(\eta^6\text{-}C_6Me_6)$, we have carried out DFT calculations on these compounds, as well as on their diamagnetic 18-electron cations $[(\eta^5\text{-}CpCONHR)Fe^{II}(\eta^6\text{-}C_6Me_6)][PF_6]$, $[(\eta^5\text{-}CpCOOR)Fe^{II}(\eta^6\text{-}C_6Me_6)][PF_6]$, and $[(\eta^5\text{-}CpCOSR)Fe^{II}(\eta^6\text{-}C_6Me_6)][PF_6]$ for the sake of comparison. Full geometry optimizations under $C_1$ symmetry have been carried out on the six complexes, and their optical transitions have been computed on the optimized geometries at the time-dependent DFT (TD-DFT) level. The comparison of the data obtained for the three 19-electron complexes gives us significant information about the influence of the functionalized cyclopentadienyl ring on the electronic structure.

## Introduction

A series of 19-electron metal sandwich complexes based on $CpFe^I(\eta^6\text{-}C_6R_6)$ (Cp = $\eta^5\text{-}C_5H_5$, R = Me or Et), called "electron-reservoir" complexes, was described in 1979.[1] These complexes were characterized by UV/vis spectroscopy, cyclic voltammetry, EPR, and Mössbauer spectroscopy, and the most commun one, $CpFe^I(\eta^6\text{-}C_6Me_6)$, was characterized by X-ray diffraction.[1] This stable 19-electron electron-reservoir complex gave rise to a particularly rich chemistry, especially in the field of electron-transfer reactions.[2] The electron-reservoir properties of this family of complexes $(\eta^5\text{-}C_5R_5)Fe^I(\eta^6\text{-}C_6R'_6)$ (R = H or Me; R′ = Me or Et) rely on the localization of the extra electron on the metal center protected by the ligand shell. Several theoretical investigations were carried out, and they all suggested that the unpaired electron is mainly localized on the metal center. Indeed, theoretical and experimental data agree on a SOMO localization following the order Fe > $-C_5R_5$ > arene, associated with a large spin density on the metal atom.[3] Even if the SOMO localization is lower in the arene ligand, several variations were made in the arene ring in order to study the stability of the complexes, and it was found that hexamethylbenzene is the most adequate arene to stabilize the 19-electron complex.[3] Besides the $C_5H_5$, $C_5Me_5$, and $C_5H_4CO_2^-$, no other variations were made to the Cp ring in order to study their influence on the stability and properties of the 19-electron complexes.

Besides electron-transfer chemistry,[1,2,3h] the $[CpFe(\eta^6\text{-arene})]$ complexes are useful for dendritic construction[3i] subsequent to photolytic ligand substitution.[3j] The electron-transfer properties can be transferred to dendrimers if the appropriate linkage is used to connect the sandwich compound to the dendrimer branches. Therefore, the amido and ester functionalities have been successfully used for this purpose, as indicated here by the thermal stability of the presently reported functional sandwich complexes of both 18- and 19-electron forms. We have also been intrigued by the variation of color of the 19-

* Corresponding authors. E-mail: d.astruc@lcoo.u-bordeaux1.fr; saillard@univ-rennes1.fr.

[†] Université de Rennes 1.

[‡] Université de Bordeaux I.

(1) (a) Astruc, D.; Hamon, J.-R.; Althoff, G.; Roman, E.; Batail, P.; Michaud, P.; Mariot, J.-P.; Varret, F.; Cozak, D. *J. Am. Chem. Soc.* **1979**, *101*, 5445. (b) Astruc, D.; Roman, E.; Hamon, J.-R.; Batail, P. *J. Am. Chem. Soc.* **1979**, *101*, 2240. (c) Hamon, J.-R.; Astruc, D.; Michaud, P. *J. Am. Chem. Soc.* **1981**, *103*, 758. (d) Astruc, D.; Hamon, J.-R.; Roman, E.; Michaud, P. *J. Am. Chem. Soc.* **1981**, *103*, 7502. (e) Hamon, J.-R.; Astruc, D.; Roman, E.; Batail, P.; Mayerle, J. J. *J. Am. Chem. Soc.* **1981**, *103*, 2431–2432. (f) Ruiz, J.; Guerchais, V.; Astruc, D. J. *Chem. Soc., Chem. Commun.* **1989**, 812. (g) Ruiz, J.; Lacoste, M.; Astruc, D. *J. Chem. Soc., Chem. Commun.* **1989**, 813.

(2) (a) Astruc, D. *Acc. Chem. Res.* **1986**, *19*, 377. (b) Astruc, D. *Chem. Rev* **1988**, *88*, 1189. (c) Astruc, D. *Bull. Soc. Chim. Jpn.* **2007**, *80*, 1658.

(3) (a) Lacoste, M.; Rabâa, H.; Astruc, D.; Le Beuze, A.; Saillard, J.-Y.; Précigoux, G.; Courseille, C.; Ardoin, N.; Boywer, W. *Organometallics* **1989**, *8*, 2233. (b) Lacoste, M.; Rabâa, H.; Astruc, D.; Ardoin, N.; Varret, F.; Saillard, J.-Y.; Le Beuze, A. *J. Am. Chem. Soc.* **1990**, *112*, 9548. (c) Ruiz, J.; Ogliaro, F.; Saillard, J.-Y.; Halet, J.-F.; Varret, F.; Astruc, D. *J. Am. Chem. Soc.* **1998**, *120*, 11693. (d) Ogliaro, F.; Halet, J.-F.; Astruc, D.; Saillard, J.-Y. *New J. Chem.* **2000**, *24*, 257. (e) Bendjaballah, S.; Boucekkine, A.; Saillard, J.-Y. *Inorg. Chim. Acta* **2005**, *358*, 1305. (f) For another DFT approach of this family of 19-electron complexes, see: Braden, D. A.; Tyler, D. R. *Organometallics* **2000**, *19*, 1175. (g) For DFT studies of other 19-electron complexes, see: Braden, D. A.; Tyler, D. R. *Organometallics* **1998**, *17*, 4060. Braden, D. A.; Tyler, D. R. *Organometallics* **2000**, *19*, 3762. (h) Desbois, M.-H.; Astruc, D.; Guillin, J.; Varret, F.; Trautwein, A. X.; Villeneuve, G. *J. Am. Chem. Soc.* **1989**, *111*, 5800. (i) Moulines, F.; Astruc, D. *Angew. Chem., Int. Ed. Engl.* **1988**, *27*, 1347. Nlate, S.; Ruiz, J.; Blais, J.-C.; Astruc, D. *Chem. Commun.* **2000**, 417. Astruc, D; Daniel, M.-C.; Ruiz, J. *Chem. Commun.* **2004**, 2637. (j) Catheline, D.; Astruc, D. J. *Organomet. Chem.* **1983**, *248*, C9.

10.1021/om7012875 CCC: $40.75 
Publication on Web 07/18/2008

electron complexes bearing these different linkages. The color change between the two easily switchable redox forms of dendritic materials can be very useful for sensing, and tuning the choice of color, which varies as a function of the link, is important in this sensor context. Since the colors are connected to the electronic structure of these redox systems, theoretical calculations concerning the spectrocopies properties are timely. In the present article, we describe the first theoretical calculations concerning the spectroscopic properties of Cp-substituted complexes ($\eta^5$-$C_5H_4X$)$Fe^I$($\eta^6$-$C_6Me_6$) (X = CONHR, COOR, COSR), including the crucial influence of the amido, ester, and thioester groups, in their two most easily accessible redox forms, $Fe^{II}$ and $Fe^I$. We report the synthesis, stability, spectroscopic properties, and theoretical calculations of three complexes of the type ($\eta^5$-$C_5H_4R$)$Fe^I$($\eta^6$-$C_6Me_6$) containing an amido, an ester, and a thioester group R directly attached to the cyclopentadienyl ring. The comparison of the properties of the three complexes, especially using UV/vis spectroscopy, will shed light on the influence of the functionalized Cp ring on the localization of the unpaired electron.

In order to provide better insight into the structural and optical properties of the three 19-electron complexes ($\eta^5$-$C_5H_4CONHR$)$Fe^I$($\eta^6$-$C_6Me_6$), **3a**, ($\eta^5$-$C_5H_4COOR$)$Fe^I$($\eta^6$-$C_6Me_6$), **4a**, and ($\eta^5$-$C_5H_4COSR$)$Fe^I$($\eta^6$-$C_6Me_6$), **5a**, we have carried out DFT calculations on these species, as well as on their diamagnetic 18-electron cations [($\eta^5$-$C_5H_4CONHR$)$Fe^{II}$($\eta^6$-$C_6Me_6$)][$PF_6$], **3**, [($\eta^5$-$C_5H_4COOR$)$Fe^{II}$($\eta^6$-$C_6Me_6$)][$PF_6$], **4**, and [($\eta^5$-$C_5H_4COSR$)$Fe^{II}$($\eta^6$-$C_6Me_6$)][$PF_6$], **5**, for the sake of comparison. Full geometry optimizations under $C_1$ symmetry have been carried out on the six compounds with the help of the ADF 2006 package.[4] In a second step, the optical transitions of the considered complexes have been computed on the optimized geometries at the time-dependent DFT (TD-DFT) level.[5]

## Results and Discussion

**1. Synthesis of the [($\eta^5$-$C_5H_4COR$)$Fe^{II}$($\eta^6$-$C_6Me_6$)][$PF_6$] Complexes and Their Reduction to 19-Electron Form.** The complex [$CpFe^{II}$($\eta^6$-$C_6Me_6$)][$PF_6$] was functionalized with amido, ester, and thioester groups directly attached to the Cp ring.

The synthesis starts with the transformation of the acid derivative [($\eta^5$-$C_5H_4COOH$)$Fe^{II}$($\eta^6$-$C_6Me_6$)][$PF_6$],[6a] **1**, to acyl chloride by refluxing complex **1** in $SOCl_2$ overnight. The resulting complex [($\eta^5$-$C_5H_4COCl$)$Fe^{II}$($\eta^6$-$C_6Me_6$)][$PF_6$], **2**, was then dissolved in dry dichloromethane and added to a dichloromethane solution of triethylamine and propyl amine (for complex **3**), phenoltriallyl dendron (for complex **4**), or decanethiol (for complex **5**). The resulting complexes were isolated as orange powders and fully characterized as 18-electron $d^6$ $Fe^{II}$ complexes (Scheme 1).

The 18-electron complexes **3**, **4**, and **5** were reduced to their 19-electron form upon reaction with the complex $CpFe^I$($\eta^6$-$C_6Me_6$), in THF, at room temperature for 5 min. The resulting 19-electron complexes **3a**, **4a**, and **5a** are stable and were characterized by UV/vis spectroscopy in order to understand the visible difference of the coloration among the three complexes. The chemical stability of the 19-electron complexes was confirmed by $^1$H NMR after a complete reduction−oxidation cycle.

**2. Cyclic Voltammetry Data.** The redox stability of the three 18-electron complexes **3**, **4**, and **5** was also studied by cyclic voltammetry in order to compare the influence, on the redox potential, of the functional group that is directly attached to the Cp ring. The three complexes present one single fully reversible redox wave in DMF. The complex **3**, which contains the amido group, is the one that presents the more negative redox potential (−1.360 V vs $FeCp_2$*) (Table 1).

**3. UV/Vis Spectroscopy.** The 19-electron complexes **3a**, **4a**, and **5a** present significantly different colors, **3a** being deep blue, **4a** turquoise blue, and **5a** deep green-gray. These differences in color are reflected in the completely different UV/vis spectra obtained for the three complexes (see Figures 1–4). This fact suggests that the functional group directly attached to the Cp ring has a significant influence on the localization of the unpaired electron. The values of absorption bands obtained for the six complexes are gathered in Table 2.

**4. Theoretical Calculations. 4.1. Geometric and Electronic Structures of the 18-Electron Cations.** The electronic structure of a typical sandwich compound such as ferrocene or $CpFe(\eta^6\text{-}C_6H_6)^+$ is that of a pseudo-octahedral 18-electron $ML_6$ species.[7] The three highest occupied MOs are nonbonding and of very large 3d(Fe) character. They constitute the so-called "$t_{2g}$" set.[7] The two lowest unoccupied MOs are metal−ligand antibonding and of dominant 3d(Fe) character. They constitute the so-called "$e_g$*" set.[7] Approximating the Cp and benzene ligands in $CpFe(\eta^6\text{-}C_6H_6)^+$ as simple circles of different sizes, the $C_{\infty v}$ pseudosymmetry can be considered for the complex. The qualitative MO diagram of $CpFe(\eta^6\text{-}C_6H_6)^+$ is sketched in Figure 5, based on the interaction between the Fe(II) metal and the $\pi$(C−C) orbitals of the benzene and $Cp^-$ ligands. The levels are labeled in both the approximate $C_{\infty v}$ (where $a_1$, $e_1$, and $e_2$ stand for $\sigma$, $\pi$, and $\delta$, respectively) and exact $C_s$ symmetries. Note that all the previous published calculations on $CpFe(\eta^6\text{-}C_6H_6)^+$ and $CpFe(\eta^6\text{-}C_6Me_6)^+$ found a very strong $C_{\infty v}$ pseudosymmetry for these compounds, i.e., an almost exact degeneracy for the levels labeled $e_1$ and $e_2$ in Figure 5.[3,7,8]

As one may expect, the major features of the $CpFe(\eta^6\text{-}C_6H_6)^+$ diagram shown in Figure 5 are maintained in the substituted **3**−**5** derivatives, although the $e_1$ and $e_2$ pseudodegeneracy is of course split by the substituent effect. The optimized geometries of the three cations are shown in Figure 6, and their major metrical and electronic data are given in Table 3. These data are consistent with those previously calculated on related species.[3,8] The MO diagrams of the three cations are shown in Figure 7. As stated above, they are related to that of their simple $CpFe(C_6H_6)^+$ relative.

A comparison of the electronic effects of the amido, ester, and thioester groups in these complexes is not straightforward. It is generally assumed that an ester group has a larger electron-withdrawing effect than an amido group, and little is known about the comparative electronic effect of a thioester group. It turns out that in the case of complex **4** the electronic effect of

(4) See for example: Fillaut, J.-L.; Andries, J.; Perruchon, J.; Desvergne, J.-P.; Toupet, L.; Fadel, L.; Zouchoune, B.; Saillard, J.-Y. *Inorg. Chem.* **2007**, *46*, 5922.

(5) (a) Vlček, A. Jr.; Záliš, S. *Coord. Chem. Rev.* **2007**, *251*, 258. (b) Barone, V.; Improta, R.; Rega, N. *Acc. Chem. Res.* **2008**, *41*, 605–616. (c) Ciofini, I.; Adamo, C *J. Phys. Chem.* **2007**, *111*, 5549, and references therein.

(6) *ADF version 2006.01*; Theoretical Chemistry Vrije Universiteit: Amsterdam, The Netherlands, SCM.

(7) van Gisbergen, S. J. A.; Snijders, J. G.; Baerends, E. J. *Comput. Phys. Commun.* **1999**, *118*, 119.

(8) (a) Román, E.; Dabard, R.; Moinet, C.; Astruc, D. *Tetrahedron Lett.* **1979**, *16*, 1433. (b) Ruiz, J.; Astruc, D *C. R. Acad. Sci. Paris, Ser. 2* **1998**, 21. (c) Ruiz, J.; Daniel, M.-C.; Astruc, D. *Can. J. Chem.* **2006**, *84*, 288.

(9) Albright, T. A.; Burdett, J. K.; Whangbo, M. W. *Orbital Interactions in Chemistry*; John Wiley and Sons: New York, 1985.

(10) Le Beuze, A.; Lissillour, R.; Weber, J. *Organometallics* **1993**, *12*, 47.

**Scheme 1. Synthesis of $[(\eta^5\text{-}C_5H_4COR)Fe^{II}(\eta^6\text{-}C_6Me_6)][PF_6]$ and Their Reduction to 19-Electron Forms**[a]

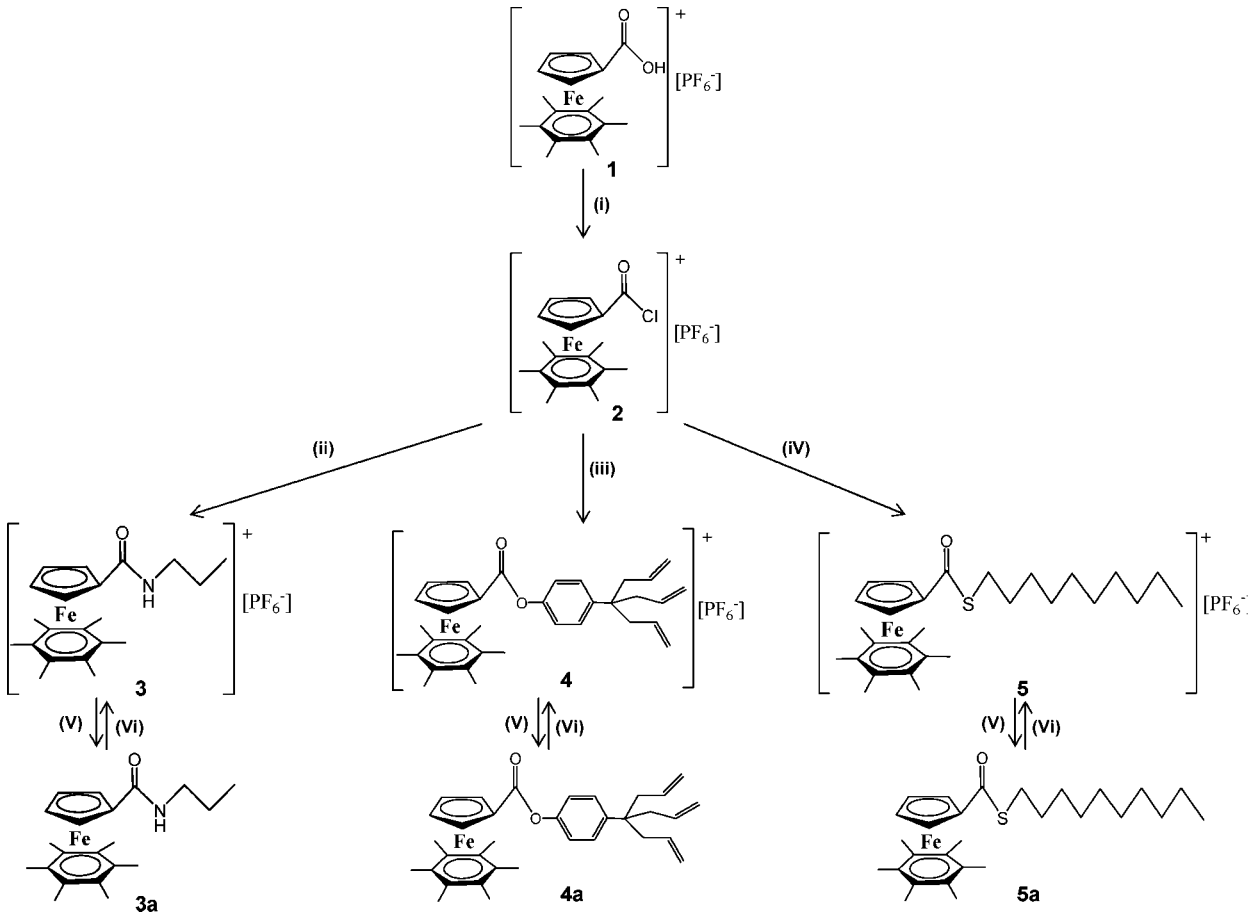


[a] (i) $SOCl_2$, reflux, 18 h; (ii) propylamine, $CH_2Cl_2$, triethylamine, rt, 4 h; (iii) phenoltriallyl dendron, $CH_2Cl_2$, triethylamine, rt, 4 h; (iv) decanethiol, $CH_2Cl_2$, triethylamine, rt, 4 h; (v) $Fe^{I}Cp(C_6Me_6)$, THF, rt, 5 min; (vi) ferricinium hexafluorophosphate, ether, rt, 5 min.

**Table 1. Redox Potentials of the Complexes $[(\eta^5\text{-}CpCOR)Fe(C_6Me_6)][PF_6]$ Obtained by Cyclic Voltammetry**

| complex | $E_{1/2}$ (V)[a] |
|---|---|
| **3** | −1.360 |
| **4** | −1.160 |
| **5** | −1.140 |

[a] $E_{1/2} = (E_{pa} + E_{pc})/2$ vs $FeCp_2^*$ (in V). Electrolyte: $[nBu_4N][PF_6]$ 0.1 M; working and counter electrodes: Pt; reference electrode: Ag; internal reference: $FeCp_2^*$; scan rate: 0.200 V $s^{-1}$; 20 °C. Solvent: dimethylformamide. Compare $[CpFe(\eta^6\text{-}C_6Me_6][PF_6]$, whose $E_{1/2}$ value is −1.425 V, to $Cp^*_2Fe$ in DMF.[6b]

the conjugated R substituent of the $CO_2R$ group is at least as important as that of the ester function. Indeed, a striking feature of **4** is that its "$t_{2g}$" set is not the highest occupied MO set as in most of the other relative compounds, but lies below a group of five MOs that are associated with $\pi$(C−C) orbitals of the conjugated R substituent. A similar but much weaker effect occurs in the thioester complex **5**, for which the "$t_{2g}$" set lies just below the HOMO, which can be identified as the highest of the $\sigma$(C−C) orbitals of the aliphatic $C_{10}H_{21}$ chain on the sulfur atom, with some metal admixture. In the cases of **3** and **5**, the electron-withdrawing effect of the amido and thioester substituents has a small stabilizing effect on the HOMO energy, which is slightly higher (−8.63 eV) in the unsubstituted $CpFe(C_6Me_6)^+$ relative. Similarly, the LUMO energies of **3**, **4**, and **5** are slightly lower than those of $CpFe(C_6Me_6)^+$, which is −6.12 eV.

**4.2. Geometric and Electronic Structures of the Neutral 19-Electron Complexes.** Calculations have shown that reducing the 18-electron $CpFe(\eta^6\text{-}C_6H_6)^+$ and $CpFe(\eta^6\text{-}C_6Me_6)^+$ complexes leads to the occupation of one of the "$e_g$*" orbitals without any significant Jahn−Teller distortion,[3,8] in agreement with all the experimental data reported on this type of complexes.[1,3] The only significant structural change is a lengthening of the Fe−C distances upon reduction, due to the occupation of a metal−ligand antibonding nature of one "$e_g$*" MO. The major computed data given in Table 3 confirm this general trend. Apart from these small differences, the optimized structures of the 18- and 19-electron complexes are very similar.

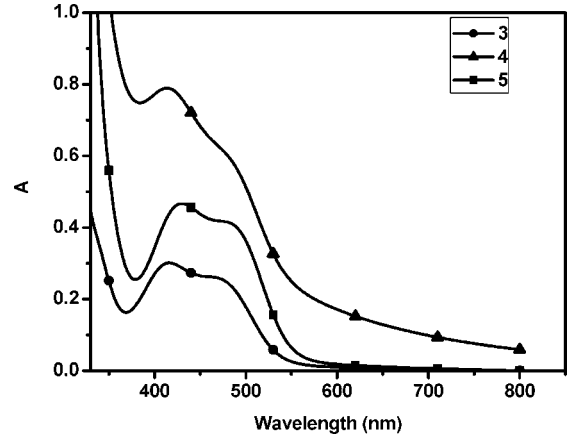


**Figure 1.** UV/vis spectra of the 18-electron complexes **3**, **4**, and **5** ($c = 2.00 \times 10^{-3}$ M in acetone).

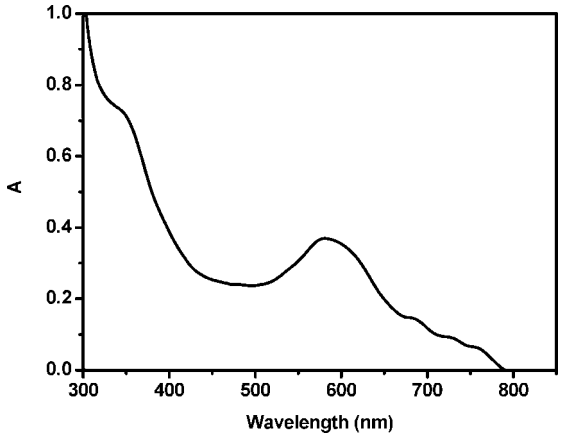


**Figure 2.** UV/vis spectrum of the 19-electron complex **3a** ($c = 3.65 \times 10^{-4}$ M in ether).

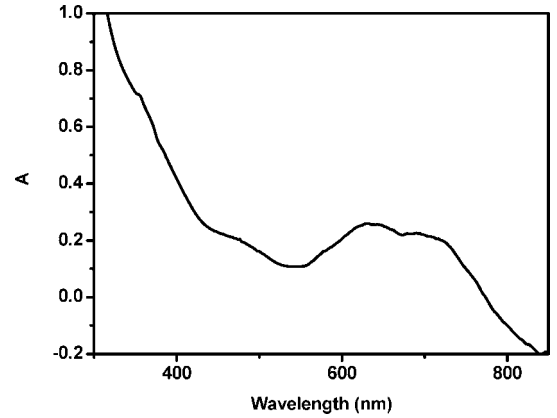


**Figure 3.** UV/vis spectrum of the 19-electron complex **4a** ($c = 4.65 \times 10^{-4}$ M in ether).

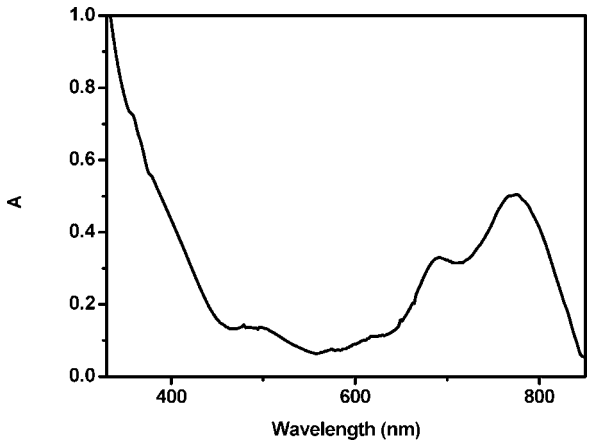


**Figure 4.** UV/vis spectra of the 19-electron complex **5a** ($c = 2.10 \times 10^{-3}$ M in ether).

The computed spin-orbital diagrams of **3a**, **4a**, and **5a** are shown in Figure 8. One can see that, contrary to the cation cases, the three highest occupied levels correspond to the "$t_{2g}$" set in the three species. The stabilization of the highest occupied ligand levels with respect to the "$t_{2g}$" set when going from **4** to **4a** should be associated with some inductive and electrostatic effects of the $CO_2R$ substituent, which stabilizes the orbitals of the electron-poor Fe(II) center in **4** and destabilizes that of the electron-rich Fe(I) center in **4a**. The effect of the substituent on the cyclopentadienyl ring is stronger for the neutral series as compared to the cationic series. In the three compounds, the

**Table 2. UV/Vis Data Obtained for the Six Complexes**

| complex[a] | | $\lambda_{max1}$ ($\varepsilon_1$) | $\lambda_{max2}$ ($\varepsilon_2$) | $\lambda_{max3}$ ($\varepsilon_3$) |
|---|---|---|---|---|
| 18-e$^-$ | **3** | 416 (151) | 462 (131) | |
| | **4** | 413 (394) | 482 (298) | |
| | **5** | 430 (233) | 484 (206) | |
| 19-e$^-$ | **3a** | 340 (2017) | 581 (1012) | |
| | **4a** | 468 (451) | 630 (561) | 690 (487) |
| | **5a** | 486 (65) | 691 (158) | 776 (240) |

[a] The UV/vis spectra were obtained in acetone for the 18-electron complexes and in ether for the 19-electron complexes.

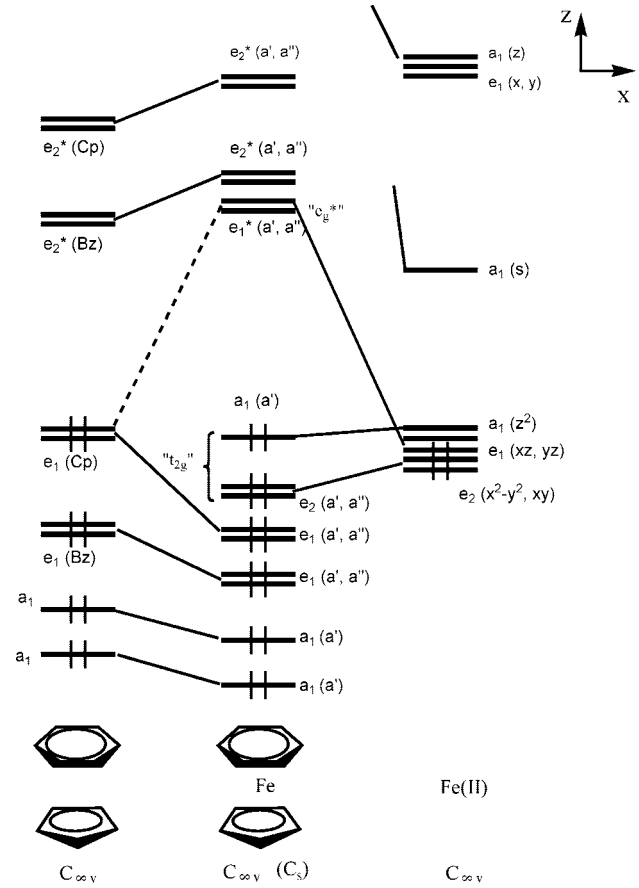


**Figure 5.** Qualitative MO interaction diagram for $CpFe(C_6H_6)^+$ ($C_{\infty v}$: pseudosymmetry; $C_s$: exact symmetry).

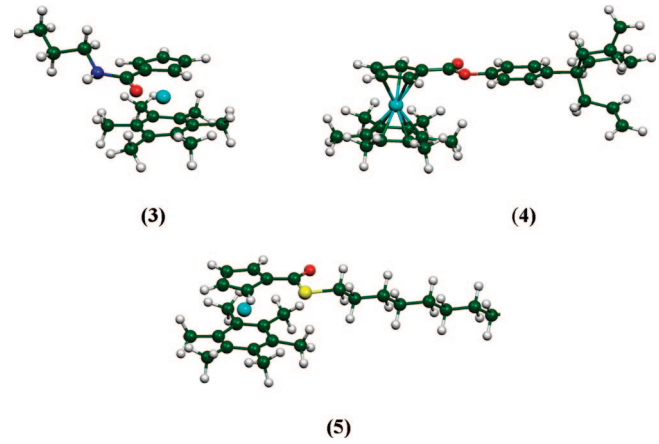


**Figure 6.** Optimized geometries of the cations **3**, **4**, and **5**.

SOMO 11a and LUMO 12a lie much lower in energy than the SOMO and LUMO of $CpFe(C_6Me_6)$, the energies of which are −2.14 and −1.56 eV, respectively. The SOMO and LUMO energy order within the series is $CpFe(C_6Me_6)$ > **3a** > **5a** ≈

**Table 3. Relevant Computed Data for the 18-Electron Cations 3, 4, and 5 and Their Reduced 19-Electron Relatives 3a, 4a, and 5a**

| | 3 | 3a | 4 | 4a | 5 | 5a |
|---|---|---|---|---|---|---|
| ionizationpotential (eV) | | 4.52 | | 4.71 | | 4.71 |
| HOMO−LUMO gap (eV) | 2.39 | | 1.29 | | 2.30 | |
| Fe−C(Cp) average (Å)[a] | 2.101 | 2.177 | 2.104 | 2.174 | 2.104 | 2.171 |
| Fe−C(Cp) range (Å) | 2.090−2.111 | 2.136−2.261 | 2.097−2.100 | 2.142−2.252 | 2.097−2.111 | 2.140−2.244 |
| Fe−C(HMB) average (Å) | 2.155 | 2.169 | 2.152 | 2.169 | 2.153 | 2.169 |
| Fe−C(HMB) range (Å) | 2.131−2.197 | 2.122−2.253 | 2.129−2.190 | 2.126−2.237 | 2.132−2.193 | 2.128−2.241 |
| C(Cp)−C(Cp) average (Å) | 1.434 | 1.434 | 1.432 | 1.433 | 1.433 | 1.433 |
| C(Cp)−C(Cp) range (Å) | 1.425−1.442 | 1.421−1.444 | 1.426−1.438 | 1.424−1.441 | 1.426−1.440 | 1.423−1.441 |
| C(HMB)−C(HMB) average (Å) | 1.434 | 1.446 | 1.435 | 1.430 | 1.434 | 1.445 |
| C(HMB)−C(HMB) range (Å) | 1.433−1.436 | 1.425−1.445 | 1.432−1.438 | 1.426−1.446 | 1.432−1.436 | 1.426−1.445 |
| Mulliken atomic spin density | | | | | | |
| Fe | | 0.90 | | 0.87 | | 0.86 |
| SOMO composition | | | | | | |
| % Fe | | 91 | | 92 | | 92 |

[a] Cp = $\eta^5$-$C_5H_4X$ (X = CONHR, COOR, COSR), HMB = $\eta^6$-$C_6Me_6$; SOMO = singly occupied molecular orbital.

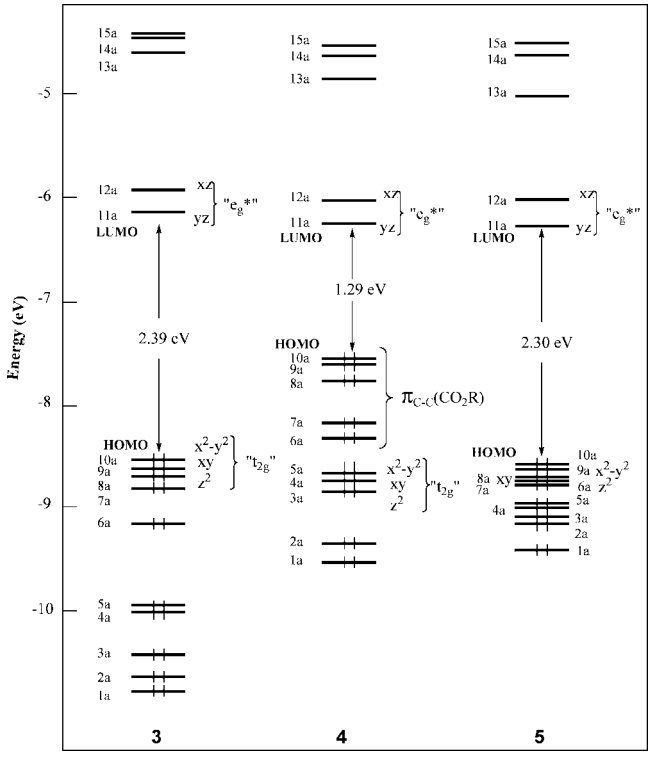


**Figure 7.** Computed MO diagrams of the 18-electron cations **3**, **4**, and **5**.

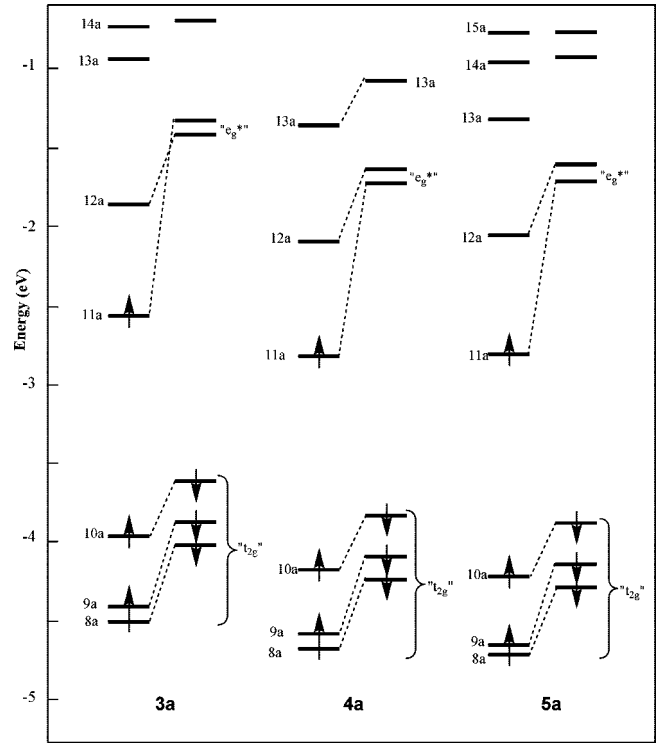


**Figure 8.** Computed level diagrams of the neutral 19-electron complexes **3a**, **4a**, and **5a**. The energies are those of spin-orbitals (spin-polarized calculations).

**4a**. This energy order follows the expected electrophilicity of the amido, ester, and thioester groups. It should be noted that in the three compounds the vacant level, which lies just above the "$e_g$*" LUMO (noted 13a in Figure 8), is derived from one of the $\pi$*(Cp) orbitals mixed in a bonding way with the $\pi$*(CO) orbital of the substituent on the Cp ring. In the case of **5a**, this accepting orbital has also some participation on the R group of the ester substituent. A plot of the three spin-up 13a spin-orbitals is shown in Figure 9. Thus, contrarily to the case of CpFe($C_6H_6$) and CpFe($C_6Me_6$), where the lowest ligand vacant orbitals are of arene major character (Figure 5), in the imido, ester, and thioester derivatives **3a**, **4a**, and **5a**, the lowest nonmetallic vacant level is localized on the substituted Cp ligand, with significant localization on the substituent.

**4.3. Computed UV/Vis Transitions of the 18- and 19-Electron Species.** For the sake of comparison, we first computed the optical transitions of the simple CpFe($\eta^6$-$C_6Me_6$)$^{0/+}$ system, which we will consider as a reference. The calculated optical spectrum of CpFe($\eta^6$-$C_6Me_6$)$^+$ is very simple, with a unique significant absorption band occurring above 200 nm. The corresponding computed maximum (233 nm) corresponds to a $\pi$(C−C)→metal("$e_g$*") transition. This value compares well to the reported experimental $\lambda_{max}$ (244 nm).[1c] The calculated optical spectrum of the 19-electron CpFe($\eta^6$-$C_6Me_6$) complex is very different. The absorption of lowest energy is computed at 792 nm and corresponds to a transition from the SOMO ("$e_g$*" component, see Figure 1) to the lowest unoccupied ligand level, which is of dominant arene character (lowest $e_2$* level in Figure 1). This is the only transition computed above 410 nm, so that it can be unambiguously indexed to the reported experimental $\lambda_{max}$ value of 684 nm.[1b] Such discrepancy between the TDDFT-computed and experimental values is not uncommon in transition-metal complexes[4] and is related to the limitations of standard TDDFT calculations in quantitatively reproducing charge-transfer transitions.[5] Three other bands are computed in the range 200−410 nm. Two of them are associated with two metal("$t_{2g}$")→ $\pi$*(C−C) at 298 and 334 nm. Thus, the ligand-to-metal transition calculated at 233 nm in the case of CpFe($\eta^6$-$C_6Me_6$)$^+$ is no longer present

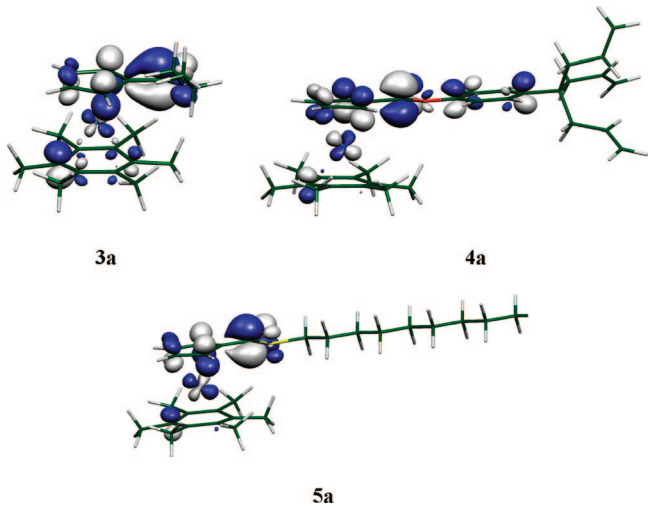


**Figure 9.** The unoccupied 13a spin-orbitals involved in the transitions of lowest energies (SOMO("$e_g$*")→ligand) computed for **3a**, **4a**, and **5a**.

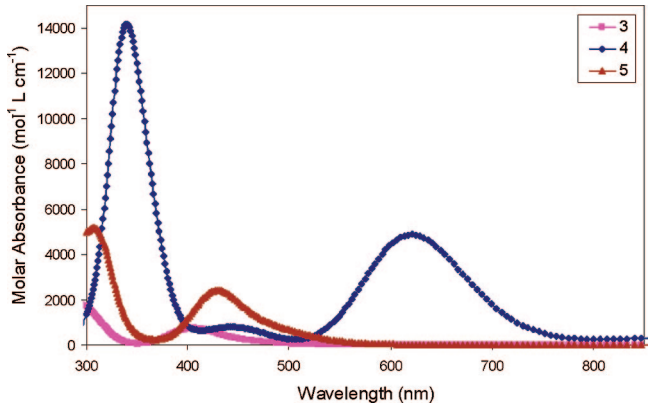


**Figure 10.** Simulated UV/vis spectra of **3**, **4**, and **5** from TD-DFT calculations.

in the computed window in the case of the neutral CpFe($\eta^6$-$C_6Me_6$) species. The third one, at 407 nm, is weaker and is a SOMO→ligand transition involving the highest arene $\pi$*(C−C) level. A similar general trend, more or less tuned by the substituent effect, is computed when comparing **3**, **4**, and **5** with their reduced relatives **3a**, **4a**, and **5a**, respectively, as described in detail below. The simulated spectra of **3**, **4**, and **5** (Figure 10) appear quite different from the experimental ones (Figure 1). Such a quantitative discrepancy is not surprising owing to the TDDFT limitations discussed above and also to the fact that our calculations do not take into account the effects of the solvent and counter anion, which are expected to be particularly important in the case of these polar species. Nevertheless, the three experimental bands reported in Figure 1 and Table 2 for each of the **3**, **4**, and **5** cations can be qualitatively assigned to the three bands of lowest energy appearing on the simulated spectra of Figure 10. In the three cases, the less energetic band is a ligand→metal ("$e_g$*") transition as in the case of CpFe($\eta^6$-$C_6Me_6$)$^+$. In the case of **3** and **5**, two other low-energy bands are also associated with ligand→metal ("$e_g$*") transitions, but involve deeper ligand levels, with in the case of **3** an additional metal ("$t_{2g}$")→ligand transition. In the case of **4**, the two other bands are ligand→ligand transitions involving the highest occupied ligand MOs, which, in that particular case, are associated with the conjugated substituent of the ester group and situated above the "$t_{2g}$" set (Figure 7).

For a better understanding of the simulated spectra, the major computed transitions and their associated oscillator strengths are reported in Table 4. As for CpFe($\eta^6$-$C_6Me_6$), the transition of lowest energy is a metal(SOMO)-to-ligand transition, the ligand level involved being the lowest vacant nonmetallic spin-orbital. However, whereas in CpFe($\eta^6$-$C_6Me_6$) this ligand level is of arene character, it is localized for the substituted cyclopentadienyl ligand in the case **3a**, **4a**, and **5a** (see discussion above and Figure 9). Although, the first transitions of the three compounds **3a**, **4a**, and **5a** are of the same SOMO("$e_g$*")→ligand nature, they differ significantly from the energetic point of view, due to very different substituent effects. As stated above, the trend in the SOMO energy is **3a** > **5a** ≈ **4a**. The trend in the energy of the 13a spin-orbital involved in the transition of lowest energy is **3a** > **4a** ≈ **5a**. Due to the presence of the substituent on the Cp ligand, the energy variation of the 13a spin-orbital is dominating. Therefore the energy of the SOMO("$e_g$*")→13a transition follows the order **4a** ≈ **5a** > **3a**. This is the major reason for their different colors. The particularly large discrepancy between experiment and theory observed for the lowest band of **4** (482 vs 621 nm) should be related to the delocalization on the $\pi$ system of its unoccupied spin-orbital involved in the transition (Figure 9), which increases the spatial range of the charge transfer.[5] As in the case of CpFe($\eta^6$-$C_6Me_6$), the other computed transitions involve the "$t_{2g}$" HOMO.

## Conclusion

Three new 18-electron complexes of the type CpFe($\eta^6$-$C_6Me_6$) containing an amido, an ester, and a thioester group directly attached to the Cp ring were synthesized and reduced to $Fe^I$ 19-electron complexes. These new 19-electron complexes are thermally stable and were characterized by UV/vis spectroscopy, showing significant differences in the spectra. Thus, it is important to consider that such functionalizations do not provoke destabilization of the 19-electron complexes. This makes feasible a strategy consisting in the synthesis of functional dendritic reservoir complexes. The influence of the functionalized Cp ring on the localization of the unpaired electron was studied by DFT calculations, and it was found that the first transitions of the three 19-electron complexes are of the same SOMO("$e_g$*")→ligand nature as in the case of CpFe($\eta^6$-$C_6Me_6$), the involved ligand level being localized on the substituted cyclopentadienyl ring, contrarily to the CpFe($\eta^6$-$C_6Me_6$) case, for which it is of arene nature. The other computed transitions involve the "$t_{2g}$" HOMO as in CpFe($\eta^6$-$C_6Me_6$). All these transitions differ significantly from the energetic point of view, due to the different substituent effects of the imido, ester, and thioester groups. This is the major reason for their different colors.

## Experimental Section

**Computational Methods.** Density functional theory (DFT) calculations were carried out on the studied compounds using the Amsterdam Density Functional (ADF) program,[6] developed by Baerends and co-workers.[11] Electron correlation was treated within the local density approximation (LDA) in the Vosko−Wilk−Nusair

(11) (a) Baerends, E. J.; Ellis, D. E.; Ros, P. *Chem. Phys.* **1973**, *2*, 41. (b) te Velde, G.; Baerends, E. J. *J. Comput. Phys.* **1992**, *99*, 84. (c) Fonseca Guerra, C.; Snijders, J. G.; te Velde, G.; Baerends, E. J. *Theor. Chim. Acc.* **1998**, *99*, 391. (d) Bickelhaupt, F. M.; Baerends, E. J. *Rev. Comput. Chem.* **2000**, *15*, 1. (e) te Velde, G.; Bickelhaupt, F. M.; Fonseca Guerra, C.; van Gisbergen, S. J. A.; Baerends, E. J.; Snijders, J. G.; Ziegler, T. J. *Comput. Chem.* **2001**, *22*, 931.

**Table 4. Relevant Computed Transitions and Their Associated Oscillator Strengths for 3, 4, and 5 and 3a, 4a, and 5a (HMB = $\eta^6$-$C_6Me_6$)**

| 3 | | | 4 | | | 5 | | |
|---|---|---|---|---|---|---|---|---|
| wavelength (nm) | oscillator strength | transitions (major components) | wavelength (nm) | oscillator strength | transitions (major components) | wavelength (nm) | oscillator strength | transitions (major components) |
| 402 | 0.009 | CONHR→"$e_g$*" | 621 | 0.067 | $\pi_{CC}$(R) →"$e_g$*" | 434 | 0.018 | COSR→"$e_g$*" |
| 279 | 0.014 | "$t_{2g}$ "→$\pi$*(HMB+Cp) | 454 | 0.004 | $\pi_{CC}$(R)→$\pi$*(HMB+Cp) | 311 | 0.056 | $\pi$(HMB+Cp)→"$e_g$*" |
| 270 | 0.027 | CONHR→"$e_g$*" | 448 | 0.004 | $\pi_{CC}$(R) →$\pi$*(HMB+Cp) | 286 | 0.043 | $\pi$(HMB+Cp)→"$e_g$*" |
| 241 | 0.087 | CONHR→"$e_g$*" | 336 | 0.075 | $\pi_{CC}$(R)→$\pi$*(HMB) | | | |
| 240 | 0.161 | CONHR→$\pi$*(HMB) | | | | | | |
| **3a** | | | **4a** | | | **5a** | | |
| wavelength (nm) | oscillator strength | transitions (major components) | wavelength (nm) | oscillator strength | transitions (major components) | wavelength (nm) | oscillator strength | transitions (major components) |
| 696 | 0.027 | "$e_g$*"→$\pi$*(Cp+CO) | 742 | 0.074 | "$e_g$*" →$\pi$*(Cp+COOR) | 736 | 0.041 | "$e_g$*"→$\pi$*(Cp+CO) |
| 545 | 0.010 | "$t_{2g}$ "→CONHR | 576 | 0.027 | "$t_{2g}$ "→COOR | 572 | 0.022 | "$t_{2g}$ "→ COSR |
| 400 | 0.006 | "$t_{2g}$ "→CONHR | 413 | 0.022 | "$t_{2g}$ "→COOR | 408 | 0.018 | "$t_{2g}$ "→ COSR |
| 344 | 0.009 | "$t_{2g}$ "→CONHR | | | | 345 | 0.025 | "$t_{2g}$ "→ "$e_g$*" |

parametrization.[12] The nonlocal corrections of Becke and Perdew were added to the exchange and correlation energies, respectively.[13,14] The numerical integration procedure applied for the calculations was developed by te Velde et al.[11e] The atom electronic configurations were described by a triple-ζ Slater-type orbital (STO) basis set for C 2s and 2p, N 2s and 2p, O 2s and 2p, and S 3s and 3p augmented with a 3d single-ζ polarization for C, N, O, and S atoms. A triple-ζ STO basis set was used for Fe 3d and 4s, augmented with a single-ζ 4p polarization function for atoms. A frozen-core approximation was used to treat the core shells up to 1s for C, N, and O, 2p for S, and 3p for Fe.[14] Full geometry optimizations were carried out using the analytical gradient method implemented by Verluis and Ziegler.[15] Spin-unrestricted calculations were performed for all the open-shell systems. The UV−visible transitions were calculated by means of time-dependent DFT (TDDFT) calculations,[7,16] at the same level of theory. Only singlet−singlet transitions, that is, spin-allowed transitions, have been taken into account. Moreover, only transitions with non-negligible oscillator strengths are reported and discussed. Representations of the molecular structures were done using MOLEKEL4.1.[17] The UV/vis spectra have been simulated from the computed TDDFT transitions and their oscillated strengths by using the SWizard program,[18] each transition being associated with a Gaussian function of half-height width equal to 3000 $cm^{-1}$.

**General Data.** Reagent-grade diethyl ether and tetrahydrofuran (THF) were predried over Na foil and distilled from sodium-benzophenone anion under argon immediately prior to use. Dichloromethane was distilled from calcium hydride just before use. The propylamine was distilled from $AlLiH_4$ just before use. All manipulations were carried out using Schlenk techniques or in a nitrogen-filled Vacuum Atmospheres drylab. The [Fe($\eta^6$-$C_6Me_6$)CpCOOH][$PF_6$] and [Fe($\eta^6$-$C_6Me_6$)CpCOCl][$PF_6$] were synthesized according to ref 6. $^1$H NMR spectra were recorded at 25 °C with a Bruker AC 300 (300 MHz) spectrometer, and $^{13}$C NMR spectra were obtained in the pulsed FT mode at 75.0 MHz with a Bruker AC 300 spectrometer. All chemical shifts are reported in parts per million ($\delta$, ppm) with reference to $Me_4Si$ (TMS). Elemental analyses were performed by the Center of Microanalyses of the CNRS at Lyon Villeurbanne, France. The mass spectra were recorded with a PerSeptive Biosystems Voyager Elite (Framingham, MA) time-of-flight mass spectrometer. All electrochemical measurements were recorded under nitrogen atmosphere. Conditions: solvent, dry dimethylformamide (DMF); temperature, 20 °C; supporting electrolyte, [$n$Bu$_4$N][$PF_6$] 0.1 M; working and counter electrodes, Pt; reference electrode, Ag; internal reference, $FeCp_2$* (Cp* = $\eta^5$-$C_5Me_5$); scan rate, 0.200 V $s^{-1}$.

**Synthesis of [Fe($\eta^6$-$C_6Me_6$)CpCONH($CH_2$)$_2$$CH_3$][$PF_6$], 3.** To a dichloromethane solution of [Fe($\eta^6$-$C_6Me_6$)CpCOCl][$PF_6$] (0.707 g, 1.44 mmol) was added 2 mL of propylamine, and the color of the solution turned from red to brown. The solution was stirred for 4 h at rt. The solvent was removed under vacuum, and the residue was dissolved in dichloromethane and washed with an aqueous solution of $HPF_6^-$. The organic layer was dried with sodium sulfate and filtrated under paper, and the solvent was removed under vacuum. Precipitation with dichloromethane/ether yielded 0.440 g of an orange powder in 60% yield.

$^1$H NMR ($CH_3COCH_3$, 300 MHz), $\delta_{ppm}$: 7.76 (s, 1H, N*H*), 5.16 and 4.94 (s, 5H, Cp), 3.33 (m, 2H, NHC$H_2$), 2.52 (s, 18H, $C_6Me_6$), 1.62 (m, 2H, NHCH$_2$C$H_2$), 0.95 (m, 3H, $CH_3$). $^{13}$C NMR ($CH_3COCH_3$, 62.90 MHz), $\delta_{ppm}$: 163.6 (C=O), 100.3 ($C_q$ of $C_6Me_6$), 85.9 ($C_q$ of Cp), 81.0 and 77.3 (*C*H of Cp), 42.7 (NH*C*H$_2$), 23.5 (NHCH$_2$*C*H$_2$), 17.0 (*C*H$_3$ of $C_6Me_6$), 11.8 (*C*H$_3$). MS (MALDI-TOF; $m/z$): calc for $C_{21}H_{30}OFe^+$ 368.31; found ($M^+$) 368.05. Anal. Calc for $C_{21}H_{30}ONFePF_6$: C 49.14, H 5.89. Found: C 48.58, H 5.77. Infrared $\nu_{C=O}$: 1666.7 $cm^{-1}$.

**Synthesis of [Fe($\eta^6$-$C_6Me_6$)CpCOOC$_6$H$_4$C(CH$_2$CH=CH$_2$)$_3$]-[$PF_6$], 4.** To a dichloromethane solution of HOC$_6$H$_4$C(CH$_2$-CH=CH$_2$)$_3$ (0.369 g, 1.62 mmol) and triethylamine (1 mL) was added a dichloromethane solution of [Fe($\eta^6$-$C_6Me_6$)CpCOCl][$PF_6$] (0.530 g, 1.08 mmol), and the color of the solution turned from red to brown. The solution was stirred for 4 h at rt. The solvent was removed under vacuum, and the residue was dissolved in dichloromethane and washed with an aqueous solution of $K_2CO_3$ and an aqueous solution of $HPF_6^-$. The organic layer was dried with sodium sulfate and filtrated under paper, and the solvent was removed under vacuum. Precipitation with dichloromethane/ether yielded 0.623 g of a brown powder in 85% yield.

$^1$H NMR ($CDCl_3$, 300 MHz), $\delta_{ppm}$: 7.39 and 7.23(d, 4H, aromatic), 5.55 (m, 1H, C*H* = CH$_2$), 5.07 (t, 2H, CH=C*H*$_2$), 5.02 and 4.91 (s, 4H, Cp), 2.44 (d, 2H, C*H*$_2$CH=CH$_2$), 2.24 (s, 18H, $C_6Me_6$). $^{13}$C NMR ($CDCl_3$, 62.90 MHz), $\delta_{ppm}$: 164.6 (*C*=O), 148.3 and 144.7 ($C_q$ of aromatic), 134.4 (H*C*=CH$_2$), 128.5 and 120.5 (*C*H of aromatic), 118.4 (HC=*C*H$_2$), 100.2 ($C_q$ of $C_6Me_6$), 85.9 ($C_q$ of Cp), 81.0 and 78.2 (*C*H of Cp), 42.7 (*C*H$_2$CH=CH$_2$), 17.5 (*C*H$_3$ of $C_6Me_6$). MS (MALDI-TOF; $m/z$): calc for $C_{34}H_{41}O_2Fe^+$ 537.52; found ($M^+$) 537.09. Anal. Calc for $C_{34}H_{41}O_2FePF_6$: C 59.83, H 6.05. Found: C 60.81, H 6.15. Infrared $\nu_{C=O}$: 1740 $cm^{-1}$.

**Synthesis of [Fe($\eta^6$-$C_6Me_6$)CpCOS($CH_2$)$_{11}$$CH_3$][$PF_6$], 5.** To a dichloromethane solution of dodecanothiol (0.286 g, 1.40 mmol) and triethylamine (1 mL) was added a dichloromethane solution of [Fe($C_6Me_6$)CpCOCl][$PF_6$] (0.462 g, 0.942 mmol), and the color

(12) Vosko, S. D.; Wilk, L.; Nusair, M. *Can. J. Chem.* **1990**, *58*, 1200.
(13) (a) Becke, A. D. *J. Chem. Phys.* **1986**, *84*, 4524. (b) Becke, A. D. *Phys. Rev. A* **1988**, *38*, 3098.
(14) (a) Perdew, J. P. *Phys. Rev. B* **1986**, *33*, 8822. (b) Perdew, J. P. *Phys. Rev. B* **1986**, *34*, 7406.
(15) Verluis, L.; Ziegler, T. *J. Chem. Phys.* **1988**, *88*, 322.
(16) Rosa, A.; Baerends, E. J.; Gisbergen, S. J. A.; van Lenthe, E.; Groeneveld, V; Snijders, J. G. *J. Am. Chem. Soc.* **1999**, *121*, 10356.
(17) Flükiger, P.; Lüthi, H. P.; Portmann, S.; Weber, J. *MOLEKEL4.1*; Swiss Center for Scientific Computing (CSCS): Switzerland, 2000−2001.

of the solution turned from red to brown. The solution was stirred for 4 h at rt. The solvent was removed under vacuum, and the residue was dissolved in dichloromethane and washed with an aqueous solution of $K_2CO_3$ and an aqueous solution of $HPF_6^-$. The organic layer was dried with sodium sulfate and filtrated under paper, and the solvent was removed under vacuum. Precipitation with dichloromethane/ether yielded 0.494 g of an orange powder in 80% yield.

$^1$H NMR ($CH_3COCH_3$, 300 MHz), $\delta_{ppm}$: 5.26 and 5.10 (s, 4H, Cp), 3.18 (t, 2H, $SCH_2$), 2.53 (s, 18H, $C_6Me_6$), 1.74 (m, 2H, $SCH_2CH_2$), 1.29 (m, 18H, $(CH_2)_9CH_3$), 0.88 (m, 3H, $CH_3$). $^{13}$C NMR ($CDCl_3$, 62.90 MHz), $\delta_{ppm}$: 190.7 ($C$=O), 101.0 ($C_q$ of $C_6Me_6$), 86.5 ($C_q$ of Cp), 82.4 and 77.4 ($CH$ of Cp), 32.9 ($SCH_2$), 23.6 ($(CH_2)_9CH_3$), 17.3 ($CH_3$ of $C_6Me_6$), 14.7 ($CH_3$). MS (MALDI-TOF; *m*/*z*): calcd for $C_{30}H_{47}OSFe^+$ 511.61; found ($M^+$) 511.21. Anal. Calc for $C_{30}H_{47}OSFePF_6$: C 54.88, H 7.22. Found: C 55.10, H 6.97.

**General Procedure for the Reduction of Complexes 3, 4, and 5.** The cationic complex was dissolved in dry THF, and $Fe^ICp(C_6Me_6)$ (1 equiv) was added. After agitation for 5 min at rt, the solvent was removed under vacuum. The 19-electron complex was extracted with dry diethyl ether.

**General Procedure for the Oxidation of Complexes 3a, 4a, and 5a.** A solution of the 19-electron complex in dry ether was added to a suspension of ferricinium (1 equiv). After agitation for 5 min at rt, the solvent was removed under vacuum, and the product was washed with pentane.

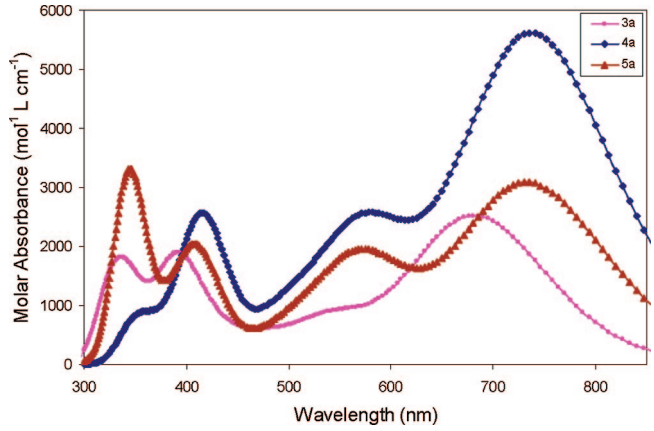


**Figure 11.** Simulated UV/vis spectra of **3a**, **4a**, and **5a**, from TD-DFT calculations.

**Acknowledgment.** We are grateful to Fundação para a Ciência e a Tecnologia (FCT), Portugal (Ph.D. grant to C.O.), the Institut Universitaire de France (I.U.F., D.A., and J.Y.S.), the CNRS, the Universities of Bordeaux 1 and Rennes 1, and ANR 06-NANO-026-01 for financial support.

OM7012875

(18) Gorelsky, S. I. *SWizard program*; http://www.sg-chem.net/ University Of Ottawa, Canada, 2007.